


RESEARCH ARTICLE

Astrocyte Responses Influence Local Effects of Whole-Brain Magnetic Stimulation in Parkinsonian Rats

Giuseppina Natale, PhD,¹ Micol Colella, PhD,² Maria De Carluccio, MSc,^{1,3} Daniele Lelli, MSc,² Alessandra Paffi, PhD,² Filippo Carducci, PhD,⁴ Francesca Apollonio, PhD,² Daniela Palacios, PhD,^{5,6} Maria Teresa Viscomi, PhD,^{5,6} Micaela Liberti, PhD,² and Veronica Ghiglieri, PhD^{6,7*} 

¹Department of Neuroscience, Università Cattolica del Sacro Cuore, Rome, Italy

²Department of Information Engineering, Electronics and Telecommunications, Sapienza University of Rome, Rome, Italy

³Department of Neurosciences and Neurorehabilitation, IRCCS San Raffaele Pisana, Rome, Italy

⁴Neuroimaging Laboratory, Department of Physiology and Pharmacology "Vittorio Erspamer", Sapienza University of Rome, Rome, Italy

⁵Department of Life Sciences and Public Health, Section of Histology and Embryology, Università Cattolica del Sacro Cuore, Rome, Italy

⁶Fondazione Policlinico Universitario Agostino Gemelli IRCCS, Rome, Italy

⁷Department of Human Sciences and Quality of Life Promotion, San Raffaele University, Rome, Italy

ABSTRACT: Background: Excessive glutamatergic transmission in the striatum is implicated in Parkinson's disease (PD) progression. Astrocytes maintain glutamate homeostasis, protecting from excitotoxicity through the glutamate–aspartate transporter (GLAST), whose alterations have been reported in PD. Noninvasive brain stimulation using intermittent theta-burst stimulation (iTBS) acts on striatal neurons and glia, inducing neuromodulatory effects and functional recovery in experimental parkinsonism.

Objective: Because PD is associated with altered astrocyte function, we hypothesized that acute iTBS, known to rescue striatal glutamatergic transmission, exerts regional- and cell-specific effects through modulation of glial functions.

Methods: 6-Hydroxydopamine-lesioned rats were exposed to acute iTBS, and the areas predicted to be more responsive by a biophysical, hyper-realistic computational model that faithfully reconstructs the experimental setting were analyzed. The effects of iTBS on glial cells and motor behavior were evaluated by molecular and morphological analyses, and CatWalk and Stepping test, respectively.

Results: As predicted by the model, the hippocampus, cerebellum, and striatum displayed a marked c-FOS activation after iTBS, with the striatum showing specific morphological and molecular changes in the astrocytes, decreased phospho-CREB levels, and recovery of GLAST. Striatum-dependent motor performances were also significantly improved.

Conclusion: These data uncover an unknown iTBS effect on astrocytes, advancing the understanding of the complex mechanisms involved in TMS-mediated functional recovery. Data on numerical dosimetry, obtained with a degree of anatomical details never before considered and validated by the biological findings, provide a framework to predict the electric-field induced in different specific brain areas and associate it with functional and molecular changes. © 2023 The Authors. *Movement Disorders* published by Wiley Periodicals LLC on behalf of International Parkinson and Movement Disorder Society.

Key Words: GLAST; glia; parkinson's disease; synaptic plasticity; transcranial noninvasive stimulation

This is an open access article under the terms of the [Creative Commons Attribution-NonCommercial-NoDerivs](https://creativecommons.org/licenses/by-nc-nd/4.0/) License, which permits use and distribution in any medium, provided the original work is properly cited, the use is non-commercial and no modifications or adaptations are made.

***Correspondence to:** Prof. Veronica Ghiglieri, San Raffaele University, Via di Val Cannuta, 247, 00166 Rome, Italy; E-mail: veronica.ghiglieri@uniroma5.it

Giuseppina Natale and Micol Colella are equally first authors; Maria Teresa Viscomi, Micaela Liberti, and Veronica Ghiglieri are equally last authors.

Relevant conflicts of interest/financial disclosures or potential

conflict of interest: The authors have no financial conflicts of interest.

Funding agencies: This work was supported by a grant from the Fresco Parkinson Institute to the New York University School of Medicine and The Marlene and Paolo Fresco Institute for Parkinson's and Movement Disorders, which were made possible with support from Marlene and Paolo Fresco (to V.G.). Università Cattolica del Sacro Cuore contributed to the funding of this research project (Linea D1 to M.T.V.).

Received: 20 March 2023; **Revised:** 11 August 2023; **Accepted:** 21 August 2023

Published online 12 September 2023 in Wiley Online Library ([wileyonlinelibrary.com](https://www.wileyonlinelibrary.com)). DOI: 10.1002/mds.29599

Transcranial magnetic stimulation (TMS) is a noninvasive brain stimulation technique,¹ generally used in the clinic as a treatment for several neurological and psychiatric disorders² and in the preclinical research setting as a neuro-investigational tool to study brain connectivity.^{3,4} TMS modulates neuronal activity by inducing an electric (E-)field⁵ that can depolarize superficial axons and activate neural networks in the cortex, therefore, achieving functional effects.^{2,6} Furthermore, if specific stimulation patterns are used (ie, repetitive TMS [rTMS] or theta-burst stimulation [TBS]), the changes in cortical excitability lead to long-lasting modifications of cerebral plasticity. The ability to induce plastic effects that persist over time suggests that these protocols enhance the brain's capacity to recover lost functions.^{7,8} rTMS induces a neuro-suppressive effect at low frequencies (below 1 Hz) and a neurogenic excitatory effect at higher frequencies (above 5 Hz). Therefore, rTMS delivered in trains of pulses is a powerful therapeutic tool for diseases caused by neuronal circuitry alterations like Parkinson's disease (PD) and other movement disorders. Relevant to PD, after a period of alternate enthusiasm for the potential of TMS to increase dopamine levels in the human brain,⁹ the idea that this neuromodulatory technique exerts therapeutic effects on motor dysfunctions has recently been revived, and groundbreaking noninvasive approaches for slowing disease progression are rapidly advancing.^{10,11} Although there is still limited information on how rTMS works at cellular and molecular levels, the study of *in vivo* effects tested in animal models helped elucidate some of these mechanisms with techniques that cannot be taken on human beings. By modulating neurotransmitters release in the rat brain,¹²⁻¹⁴ rTMS mediates neuroplasticity, activates specific brain regions, and increases the expression of selective genes.¹⁵⁻¹⁸ Besides neurons, non-neuronal cells respond to electrical activity directly or indirectly, making them intriguing candidates to mediate the effects of TMS.¹⁹⁻²³ Specifically, astrocytes are critical regulatory cells able to react with structural and functional changes to a variety of insults that alter cellular and extracellular environments and are likely to be the key players in the TMS-induced brain changes.²⁴ Astrocytes maintain glutamate homeostasis, support normal neuronal function, and protect from neuronal excitotoxicity by controlling extracellular glutamate through the astrocytic glutamate transporter-1 (GLT1), and glutamate-aspartate transporter (GLAST).^{24,25} Accordingly, alterations in GLT1 and/or GLAST have a causal role in the inefficient control of astrocytic glutamate uptake function in several central nervous system (CNS) disorders,²⁶ such as PD.^{27,28} Impaired glutamate uptake entails neuropathological consequences such as alterations of synaptic neurotransmission, neuronal excitotoxicity, astro- and microgliosis, and neurodegeneration.²⁹ Therefore, correcting the altered functions of astrocytes is an appealing strategy for treating neurodegenerative disorders such as PD.

Here, we tested the hypothesis that intermittent TBS (iTBS), previously shown to rescue striatal plasticity, functional connectivity, and control of glutamatergic tone in a 6-hydroxydopamine (6-OHDA)-lesioned PD model,^{13,14,30} may exert these effects by modulating astrocytic functions. Specifically, we evaluated the potential of TMS of restoring the impaired ability of glial cells to regulate extracellular glutamate and its effectiveness on motor recovery.

Given that PD-related alterations of plasticity are primarily observed in specific brain areas, we investigated the E-field induced in the striatum and other areas by a whole-brain magnetic stimulation approach to test whether local glial cell populations influence a possible regional-specific effect. To this aim, our investigation was paralleled by numerical dosimetry on an anatomically detailed rat model taken from the Information Technologies in Society (IT²S) ViZOO population,³¹ whose brain was substituted by the highly detailed 3DWaxholm space-atlas, counting more than 200 between brain structures and functional areas.^{32,33} We developed a hyper-realistic biophysical computational model as a framework to link the estimated TMS-induced E-field with the biological findings that may guide the implementation of TMS coils for preclinical research.

Materials and Methods

Extended methods may be found in the Supplementary Data file.

Biophysical Computational Model

The Numerical Model: TMS Coil and Realistic Rat

The experiments performed here and in previous papers^{13,14} were computationally reproduced in the Sim4Life environment (Zurich MedTech AG, Zurich) by considering the model of the 70 mm figure-of-eight stimulating coil and the male Wistar rat model taken from the ViZOO population (ie, the big rat).³¹ The coil model consisted of two connected co-planar windings made of a wire with a dimensionless cross-section,^{34,35} whereas the rat brain model was ad hoc modified, replacing it with the open-source Waxholm space atlas (RRD: SCR_017124),^{32,33} a highly detailed three dimensional (3D) digital brain atlas. This allowed us to integrate an accurate model of the entire rat body, with a separate representation of up to 220 specific brain areas, including the targets of this study, such as the hippocampus, the striatum, and the cerebellum, and their subregions, as in Figure 1A where the full model, with the coil placed over the bregma of the 3D virtual rat, is shown.

The Electromagnetic Simulation Setup

The TMS current pulse was approximated as a continuous sinusoid at a frequency of 3 kHz,³⁶⁻³⁹ with an intensity extracted from the measured data reported in the coil datasheet (ie, 3.7 kA). At such frequency, the conductivity

values assigned to each tissue were taken from the Low Frequency (LF) IT'IS database, particularly the value of 0.234 S/m, associated with the brain, was assigned to all the regions, except for the cerebellum ones that have a conductivity of 0.66 S/m. The electromagnetic (EM) solution was obtained using the low-frequency magneto quasi-static solver of the simulation software Sim4Life (Zurich MedTech, AG) (Supplementary Figs. S1–S3). The robustness of the results against possible misplacements of the coil (ie, shifting or tilting) was evaluated and is reported in the Supporting Data (Supplementary Figs. S4 and S5).

Experimental Model

Animal Preparation, Motor Behavioral Testing, and TMS Treatment In Vivo

Unilateral medial forebrain bundle injection of saline (sham-operated [CTRL] $n = 10$ rats) or 6-OHDA (fully

lesioned [FL] $n = 18$ rats) was done by stereotaxic surgery.⁴⁰ The Stepping test and the CatWalk quantitative gait analysis were used as previously reported.¹³ CTRL and FL animals (5–7 animals/group) were tested before stimulation. Therefore, animals were subjected to a single placebo or iTBS session in awake non-anesthetized condition,¹³ as previously reported. Animals were then tested again 80 minutes after acute iTBS sessions.

Immunofluorescence and Confocal Microscopy

Brains slices of CTRL and 6-OHDA groups, treated with either acute placebo stimulation (FL) or iTBS (FL + iTBS), were obtained and processed as previously described.¹³

Quantitative Analysis of Glial Cell Activation

Microglia and astrocyte cell counting was performed offline on the striatum, hippocampus, and cerebellum,

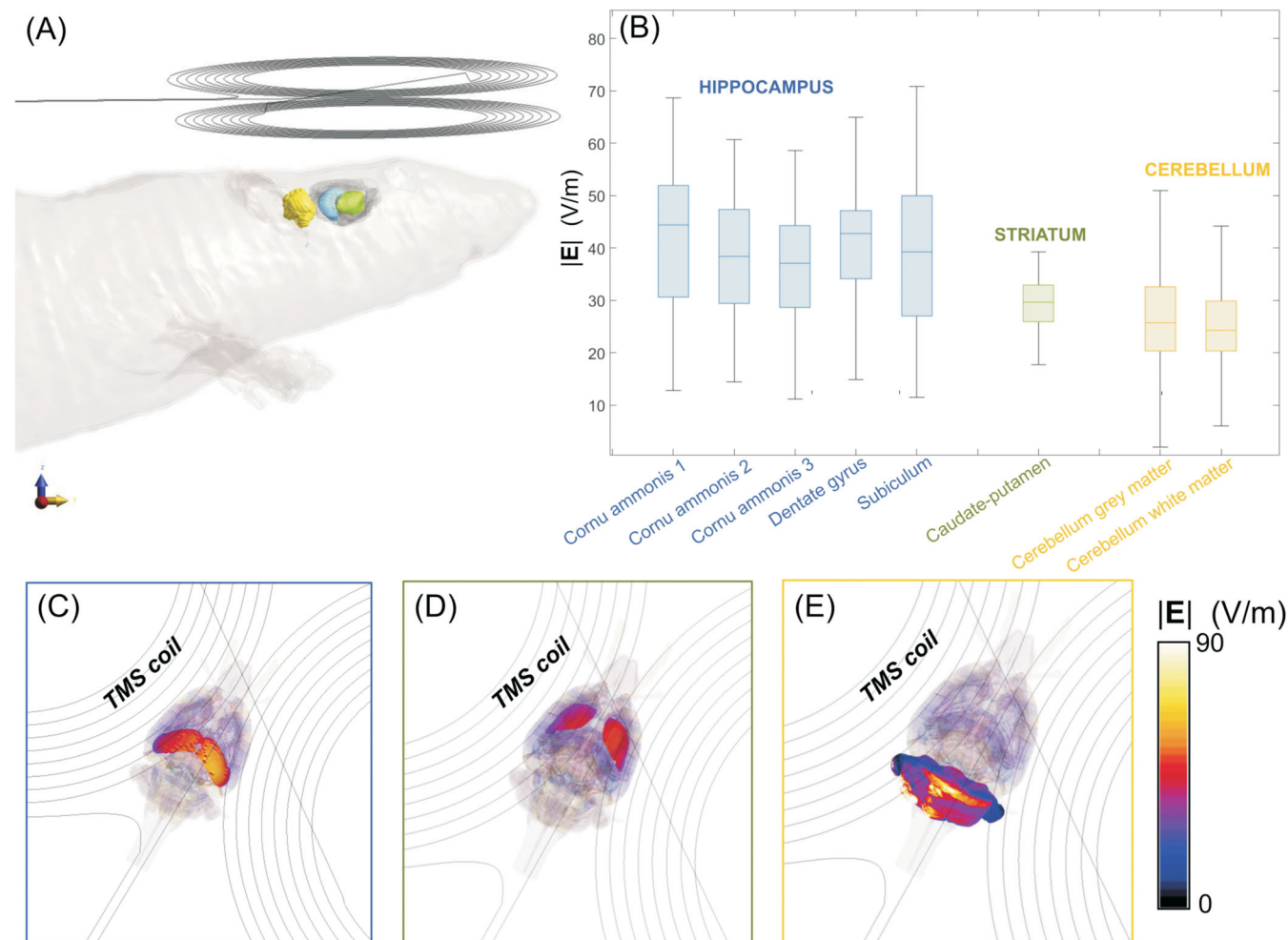


FIG. 1. Simulated induced electric (E)-field inside the animal's brain. (A) Model detail of hippocampus, striatum, and cerebellum. (B) Box plot of the induced E-field intensities in the single sub-areas of hippocampus, striatum, and cerebellum. The box represents the interquartile range, and the whiskers represent the most extreme data point not considered an outlier. To compare the dispersion of the induced E-field values among the three areas, the quartile coefficient of dispersion, defined as $QCD = \frac{(E_{75} - E_{25})}{(E_{75} + E_{25})}$ was calculated. This quantity provides a robust measure of the spread of the E-field intensity distribution in each region⁴³ and showed similar dispersion in the hippocampus and cerebellum (0.23 and 0.21, respectively), twice as in the striatum ($QCD = 0.12$). Induced E-field intensity maps on the surface of the hippocampus (C), striatum (D), and cerebellum (E).

as already reported.⁴¹ For analysis, $n = 3$ animals/group, and, for each animal, 5 sections regularly spaced rostro-caudally were used.

Sholl Analysis of Glial Cells

Sholl analysis of astrocytes and microglia was performed by NeuroLucida 7.5 (MicroBright-Field, Williston, VT, USA). Fifty cells per animal ($n = 3$ animals/group; 5 sections/animal) were randomly selected and included for analysis. Cell body area, number of intersections (the number of glia branches that intersect/cross the radius), and total length of all processes were measured.⁴²

Quantitative Real-Time Reverse Transcription Polymerase Chain Reaction

RNA was extracted from the dorsolateral striatum (CTRL $n = 7$; FL $n = 6$ and FL $n = 6$ rats) by using Total RNA Purification Kit from Norgen Biotek (Thorold, ON, Canada) and retro-transcribed using the PrimeScript RT Reagent TAKARA kit (Takara Bio, Saint-Germaine-en-Laye, France) following manufacturer indications. Quantitative polymerase chain reaction (PCR) was performed using the TB Green Premix Ex Taq TAKARA kit reagents. The primers used are listed in Table 1. Gene expression was normalized to the expression of *Actb*. Fold change was determined by using the $\Delta\Delta C(t)$ method.

Statistical Analyses

Statistical analyses were carried out using GraphPad Prism 6.0 (GraphPad software for Science, San Diego, CA, USA). All quantitative analyses were conducted blind to the animal's experimental condition.

Semiquantitative data were analyzed by using an unpaired Student's *t* test. For Sholl analysis, all experimental groups were compared using two-way ANOVA by Tukey's post hoc test. Quantitative reverse transcription (qRT)-PCR data were analyzed by using an unpaired Student's *t* test. For behavioral analyses, comparisons were done using two-way-ANOVA followed by Šídák's multiple comparisons test for the CatWalk and paired Student's *t* test for the Stepping test. All values are expressed as mean \pm standard error of the mean. Values of $P \leq 0.05$ were considered statistically significant.

TABLE 1 Primers used and designed by NCBI Primer-Blast program

Gene	Reverse	Forward
<i>Actb</i>	5'-CTACGTACATGGCTGGGGTG-3'	5'-GAACCCTAAGGCCAACCGTG-3'
<i>Cfap</i>	5'-TGTAGCTAGCAAAGCGGTCA-3'	5'-GTCTCGAATGACGCCTCCAC-3'
<i>Glast</i>	5'-ATACGGTCGGAGGGCAAATC-3'	5'-TGCCTTTGTGCTACTCACCG-3'
<i>Glt1</i>	5'-TCGCCAGAGTTGCTGTAAGG-3'	5'-TACAGCCCTTTACGAAGCCG-3'

Results

Numerical Estimation of the TMS-Induced Electric Field Inside the Animal's Body

The magnetic flux density (B-field) generated by the TMS coil and the induced E-field were estimated. Supplementary Figure S3A shows that with the coil placed as in the in vivo treatment, a maximum coupling between the coil and the animal occurred. Hence, the induced E-field focused on the head and the initial tract of the spinal cord (Supplementary Fig. S3B), reaching values above 50 V/m in the brain area and scalp, whereas it remained negligible along the rest of the spinal cord. This ensured a good exposure of the brain area and a reduced risk of unwanted stimulation of non-targeted areas.

The distribution of the E-field induced inside the single subregions of the target areas of hippocampus (ie, cornu ammonis, dentate gyrus, and subiculum), striatum (ie, caudoputamen), and cerebellum (ie, grey and white matter) is reported as boxplot in Figure 1B. The hippocampal areas are all exposed to intensities above 10 V/m, reaching a maximum of 70 V/m in the subiculum. Because of its extension in the coronal direction, both toward the interaural line (further from the coil) and toward the cortex (closer to the coil), as shown in Figure 1C, the values estimated inside the hippocampus are dispersed, with a maximum interquartile range (IQR) of 23 V/m around a mean value of 40 V/m. Conversely, the striatum has a more compact geometry. It almost entirely lies equally distant from the coil, hence, it experiences intensities slightly lower than the hippocampus, with a mean value $E_{\text{mean}} = 29.5$ V/m, and ranging between 18 V/m and 40 V/m (Fig. 1D). In the cerebellum, the induced E-field reaches intensities above 50 V/m, with peaks up 85 V/m (Fig. 1E), estimated as the 99.9th percentile of the distribution, but it has the lowest values for E_{mean} (25 V/m) and the 25th percentile of the distribution (20 V/m). As a whole, the E-field distribution induced in the cerebellum is the most spread.

To compare the dispersion of the induced E-field values among the three areas, the quartile coefficient of dispersion, defined as $QCD = \frac{(E_{75} - E_{25})}{(E_{75} + E_{25})}$ was calculated. This quantity provides a robust measure of the spread

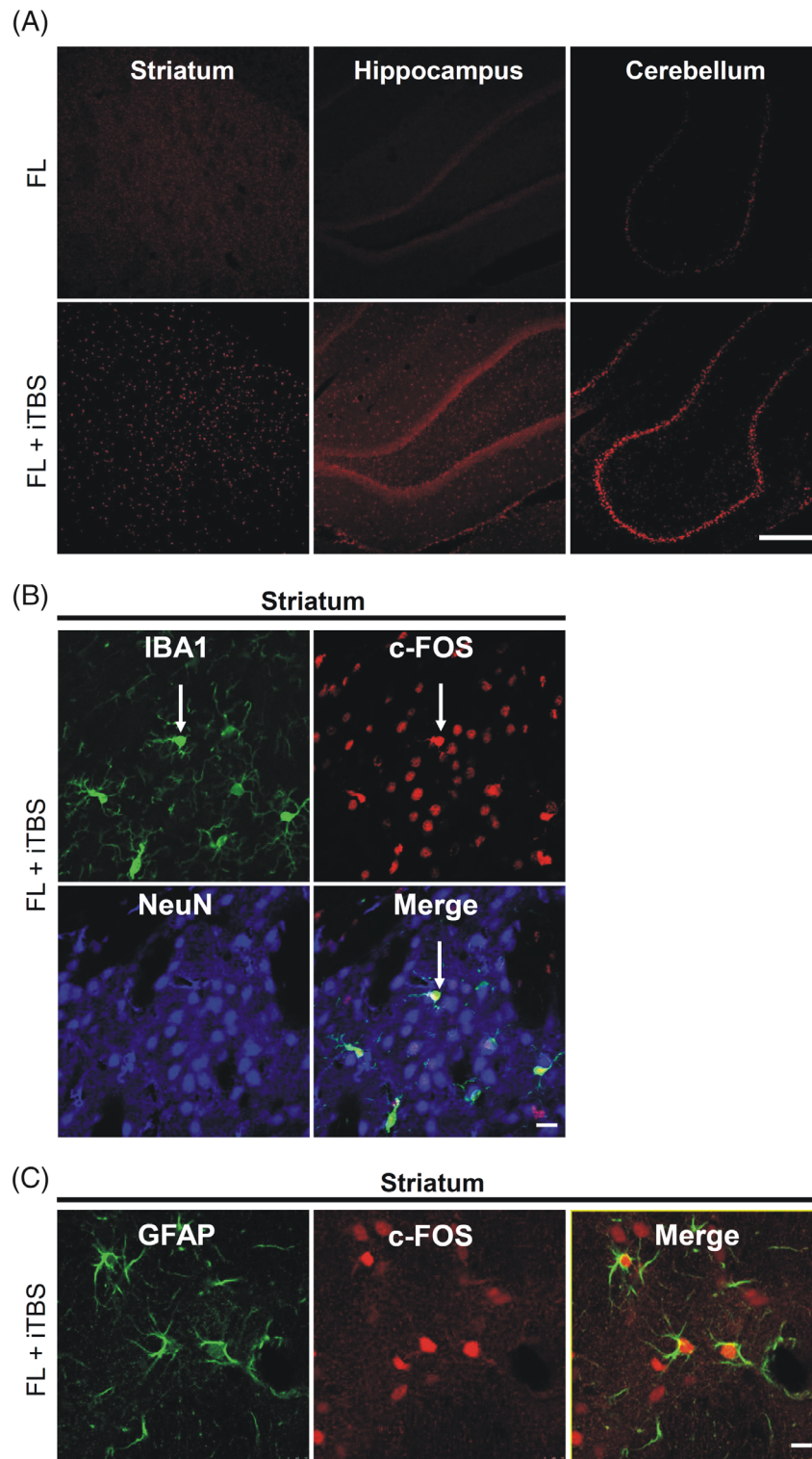


FIG. 2. Effects of intermittent theta-burst stimulation (iTBS) on c-FOS immunoreactivity in different brain structures of fully lesioned animals. (A) c-FOS immunolabeling confocal images in the dorsolateral striatum ipsilateral to the lesion side, hippocampus, and cerebellum in fully-lesioned (FL) animals and FL animals after a single session of iTBS animals (FL + iTBS). Scale bar, 100 μ m. (B) IBA1, c-FOS, and NeuN triple-labeling confocal images at the level of the dorsolateral striatum ipsilateral to the lesion side in FL + iTBS animals showing the c-FOS co-localization with both IBA1⁺ microglia (arrow) and NeuN⁺ neurons (arrowhead). Scale bar, 15 μ m. (C) Glial fibrillary acidic protein (GFAP) and c-FOS double-labeling confocal images at the level of the dorsolateral striatum ipsilateral to the lesion side in the FL + iTBS group showing the c-FOS co-localization with GFAP⁺ astrocytes. Scale bar, 15 μ m.

of the E-field intensity distribution in each region⁴³ and showed similar dispersion in the hippocampus and cerebellum (0.23 and 0.21, respectively), twice as in the striatum (QCD = 0.12).

All the brain areas have been estimated to experience induced E-field intensities comparable to those estimated for TMS application in humans, able to alter cortical activity,^{5,36-38,44} where the coil is fed at 50%–80% of the maximum stimulation output (MSO) (ie, 100%–120% of the resting motor threshold).

c-FOS Immunoreactivity Is Increased in Predicted Responsive Brain Areas

To validate the E-field distribution data, we first assessed the c-Fos induction, a marker of neuronal activity that changes in response to magnetic stimulation,⁴⁵ in the cerebellum, the striatum, and the hippocampus. These latter two areas are critically affected in PD.⁴⁶

Confocal analysis of c-FOS staining shows that in parkinsonian rats exposed to placebo stimulation (FL), c-FOS immunoreactivity was relatively low in all the brain areas of interest (Fig. 2A). Conversely, in parkinsonian rats exposed to acute iTBS (FL + iTBS) c-FOS immunostaining was diffuse in all of the brain areas analyzed (Fig. 2A).

It has been shown that glial cells are responsive to TMS-induced quantities,⁴⁷ and the regulation of their biology has been suggested as a possible mechanism for TMS effectiveness.²⁰ Therefore, focusing on the striatum, the brain area mainly affected in PD, we checked the responsiveness of the different glial populations to TMS fields, with a particular interest in astrocytes. Notably, the phenotypic characterization of the different cellular populations of the striatum in the FL + iTBS group resulted in a robust induction of c-FOS immunostaining in neurons (Fig. 2B), as already shown,¹³ but also in Iba-1⁺ microglia (Fig. 2B) and markedly in glial fibrillary acidic protein (GFAP)⁺ astrocytes (Fig. 2C). To examine induction of c-FOS in neurons¹³ we performed double labeling of c-FOS with DARPP32 or choline acetyltransferase or parvalbumin. Confocal analysis confirmed that c-FOS was mainly expressed by striatal spiny projection neurons, whereas it was lacking in local interneurons (Supplementary Fig. S6).

Striatal Astrocytes and Microglia Are Selectively Responsive to a Single Session of iTBS

We, then, investigated the effects of iTBS on glial responses. Regarding astrocytes, the FL group presented a higher number of GFAP⁺ cells compared to unlesioned rats (CTRL) ($P < 0.01$) (Fig. 3A,B). Of note, the 6-OHDA lesion did not significantly affect the

number of GFAP⁺ cells in the hippocampus ($P = 0.076$) and the cerebellum ($P = 0.078$) (Supplementary Fig. S7A,B). Additionally, this effect was only observed after the 6-OHDA lesion, as no astrocyte reactivity changes are observed in CTRL rats subjected to active iTBS as previously reported.¹³

Following acute iTBS, the number of GFAP⁺ cells in parkinsonian animals (FL + iTBS) was significantly lower than in FL ($P < 0.01$) and higher than in CTRL ($P < 0.05$) (Fig. 3A,B).

The analysis of striatal microglia shows that FL rats presented a number of IBA1⁺ cells higher than in CTRL group ($P < 0.01$), as previously reported.¹³ However, like astrocytes, no significant effects of the lesion were observed in the hippocampus ($P = 0.11$) and cerebellum of FL group compared to CTRL ($P = 0.08$) (Supplementary Fig. S7A,B).

Interestingly, further differences between the two glial populations were observed within the striatum. The effect of iTBS after 6-OHDA lesion on microglia was less intense than in astrocytes, with the FL + iTBS group showing a slightly lower number of IBA1⁺ cells than in the FL group ($P < 0.05$), but significantly different from the CTRL ($P < 0.01$) (Fig. 3A,B).

In addition to their number, dopamine denervation and iTBS treatment also changed the morphology of reactive astrocytes and microglia. In the striatum of FL group, GFAP⁺ cells showed a higher degree of complexity compared to CTRL, presenting a larger cell body ($P < 0.001$), as well as longer ramifications (CTRL vs. FL $P < 0.0001$) and increased number of intersections (CTRL vs. FL $P < 0.0001$), particularly at the radii close to the cell bodies (Fig. 3C). Conversely, in FL + iTBS group, GFAP⁺ cells presented a demerified morphology compared to those of FL, showing significantly smaller cell body ($P < 0.001$) and shorter and less ramified processes (Fig. 3C). Moreover, Sholl analysis of microglia of FL group presented increased soma area compared to CTRL group ($P < 0.0001$) (Fig. 3D), and although the number of intersections at the radii closer to the soma were changed (10–20 μm $P < 0.0001$; 30 μm $P < 0.01$), the processes lengths were only significantly altered at 10 μm (10 μm $P < 0.001$) (Fig. 3D). In FL + iTBS animals, the soma area was smaller than that of FL ($P < 0.001$) (Fig. 3D), but the number of intersections and the processes length were not significantly different (Fig. 3D).

Acute iTBS Modulates the CREB Pathway, Increases Striatal GLAST Expression, and Improves Functional Recovery

We then asked whether the 6-OHDA-induced astrocytic response was because of impaired expression of *Glut* and *Glt1*, which play a crucial role in removing excessive extracellular glutamate, a condition associated

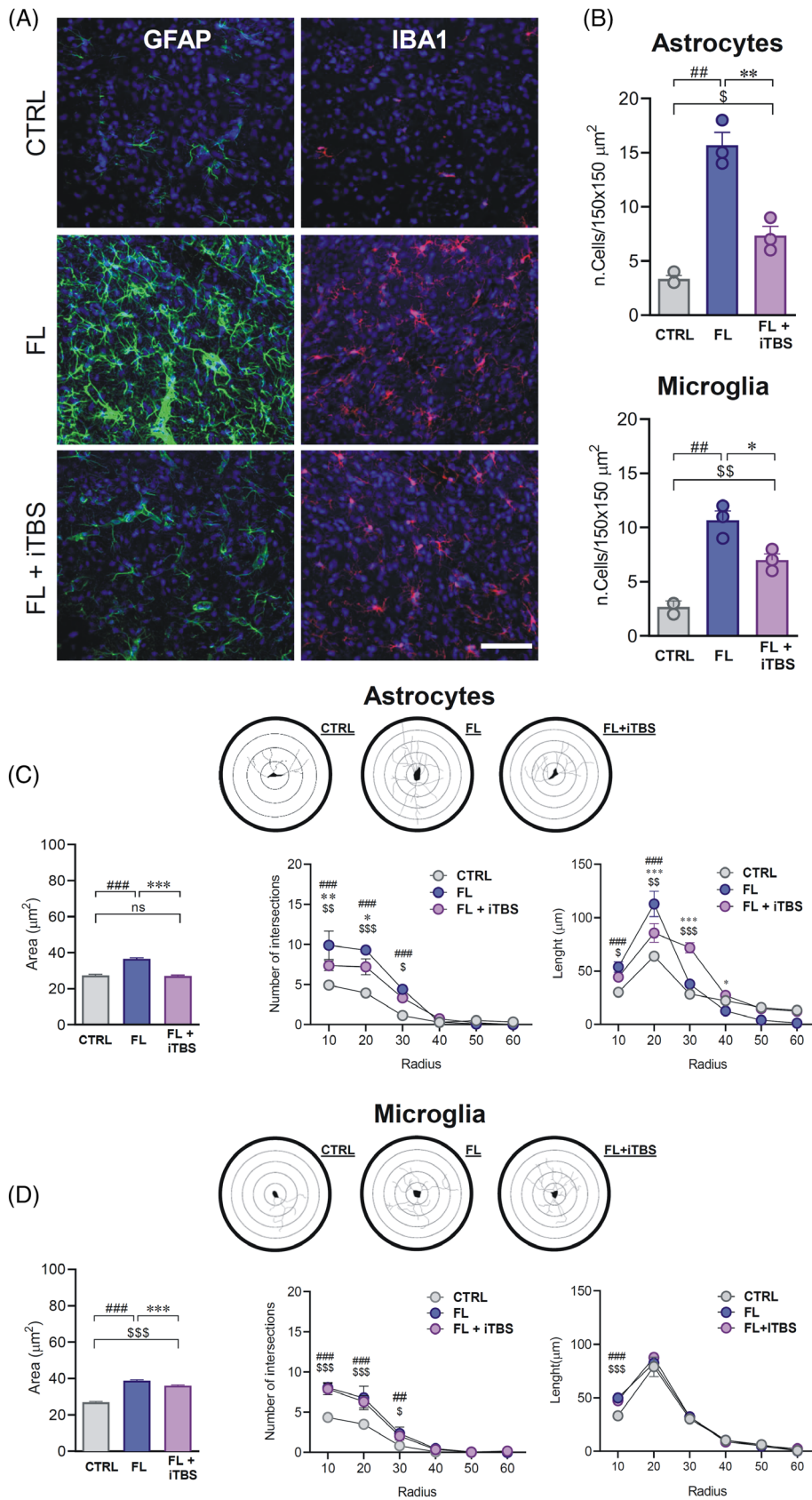


FIG. 3. Legend on next page.

with PD¹⁴ and other pathological conditions.⁴⁸ As shown in Figure 4A, *Glast* mRNA levels decreased significantly in FL animals compared to CTRL ($P < 0.01$) and rose significantly in FL + iTBS compared to FL ($P < 0.05$), reaching CTRL levels. Conversely, *Glt1* mRNA levels in FL animals did not change significantly from CTRL, and displayed a high variability after the iTBS treatment (Fig. 4A).

Considering the exclusive effects of iTBS on GLAST level, we explored the co-localization of GLAST and GFAP using an immunofluorescence assay and evaluated the Manders' correlation coefficient (MCC) (see Supporting Data) between the two markers. Notably, we found that in the CTRL group, GLAST immunostaining was detectable in GFAP⁺ cells (Fig. 4B), whereas it was absent in GFAP⁺ cells of the FL group (Fig. 4B) and similar to CTRL following iTBS treatment (FL + iTBS). The MCC analysis confirmed that the value in CTRL was 0.626, showing an overlapping between GLAST and GFAP. Conversely, a lower degree of co-localization between GLAST and GFAP was found in the FL group (0.362), whereas in the FL + iTBS group, the MCC value was 0.578, returning at control levels.

As GLAST/GLT-1 expression is negatively regulated by the CREB pathway,⁴⁹ we measured phospho-CREB (ph-CREB) levels in GFAP⁺ cells in different conditions. In the striatal GFAP⁺ cells of the FL group, ph-CREB levels increased as compared to CTRL animals ($P < 0.001$) (Fig. 4D). Notably, and in striking contrast with the GLAST expression, ph-CREB immunostaining was lower in GFAP⁺ cells of the FL + iTBS group than in FL animals ($P < 0.001$) (Fig. 4C,D), with values similar to the CTRL group ($P = 0.16$) (Fig. 4C,D).

Finally, to assess the effects of iTBS on the recovery of motor control, we subjected the rats to the analysis of gait using the CatWalkXT system and to the Stepping test. Among the gait parameters extracted from the automated analysis, we observed that the step cycle (the time between two consecutive initial contacts of the same paw) was reduced in the FL group for both the right and the left paws ($P < 0.01$) with respect to CTRL. Accordingly, the stride length, defined as the distance between successive placements of the same paw, was also found to be lower in the FL group than in CTRL ($P < 0.05$). In line with previous findings reporting a recovery of step sequence pattern in TMS-exposed animals,¹³ parkinsonian animals exposed to

iTBS showed a recovery of both step cycle and stride length ($P < 0.05$ and $P < 0.001$, respectively) of the paws contralateral to the lesion side (Fig. 4E).

Furthermore, we estimated forelimb akinesia and limb-use asymmetry through the Stepping test. Post-stimulation comparisons of contralateral/ipsilateral steps ratios revealed that after iTBS FL rats used significantly more the contralateral (impaired) forelimb than before the stimulation ($P < 0.01$) (Fig. 4F), as previously reported.¹³

Discussion

In this study, we demonstrated that the effects of iTBS are prominent in CNS structures significantly impaired in PD, such as the striatum and hippocampus, and that, selectively in the striatum, a greater and more complex response is observed in astrocytes over microglia. In the parkinsonian condition, astrocyte reactivity was associated with the reduced expression of the glutamate transporter GLAST, critically involved in the astrocytes' ability to counteract hyperglutamatergic state in corticostriatal synapses.

Our data support the notion that nigrostriatal dopamine loss affects both neurons and glial cells. In fact, it is well established that dopamine denervation brings a reduced inhibitory control of glutamatergic neurotransmission.^{14,50,51} Such an increase in extracellular glutamate, besides perturbing the induction of corticostriatal plasticity,⁵² is a potent trigger for astrocyte activation.²⁸ Therefore, dopamine D2 receptors, besides controlling the activity-dependent release of glutamate in corticostriatal neurons through multiple mechanisms (including endocannabinoid production)^{53,54} also modulate glutamate homeostasis in astrocytes, which express dopamine and CB1 receptor subtypes as well.^{55,56} Therefore, we speculate that in our model the lack of dopaminergic control over glutamate release engages astrocytes reactivity, ultimately leading to synaptic plasticity dysfunctions.

Because plasticity is lost in both the striatum and hippocampus after nigrostriatal denervation,⁴⁶ we analyzed the glial reactivity in these areas. Our results show a robust increase in both astrocyte and microglia reactivity in the striatum of parkinsonian rats, an effect that was not observed in the hippocampus.

FIG. 3. Effects of intermittent theta-burst stimulation (iTBS) on striatal astrocytes and microglia responses induced by the 6-hydroxydopamine lesion. (A) Lower magnification of merged confocal images of glial fibrillary acidic protein (GFAP) (green) and IBA1 plus DAPI counterstaining (blue) in the different experimental conditions. Scale bar, 25 μm . (B) Bar graphs of the quantification of GFAP⁺ and IBA1⁺ cells in the striatum of sham operated (CTRL), fully lesioned (FL), and FL + iTBS animals ([§] $P < 0.05$, ^{##,§§} $P < 0.01$). (C) Box plot of soma area quantification, number of intersections, and length of processes of GFAP⁺ cells in the different experimental conditions and representative images of three dimensional (3D) reconstructed astrocytes phenotypes ([§] $P < 0.05$, ^{§§} $P < 0.01$, ^{###,***,§§§} $P < 0.001$). (D) Box plot of soma area quantification, number of intersections, and length of processes of IBA1⁺ cells in the different experimental conditions and representative images of 3D reconstructed microglia phenotypes ([§] $P < 0.05$, ^{##} $P < 0.01$, ^{###,***,§§} $P < 0.001$). Data are reported as mean \pm standard error of the mean.

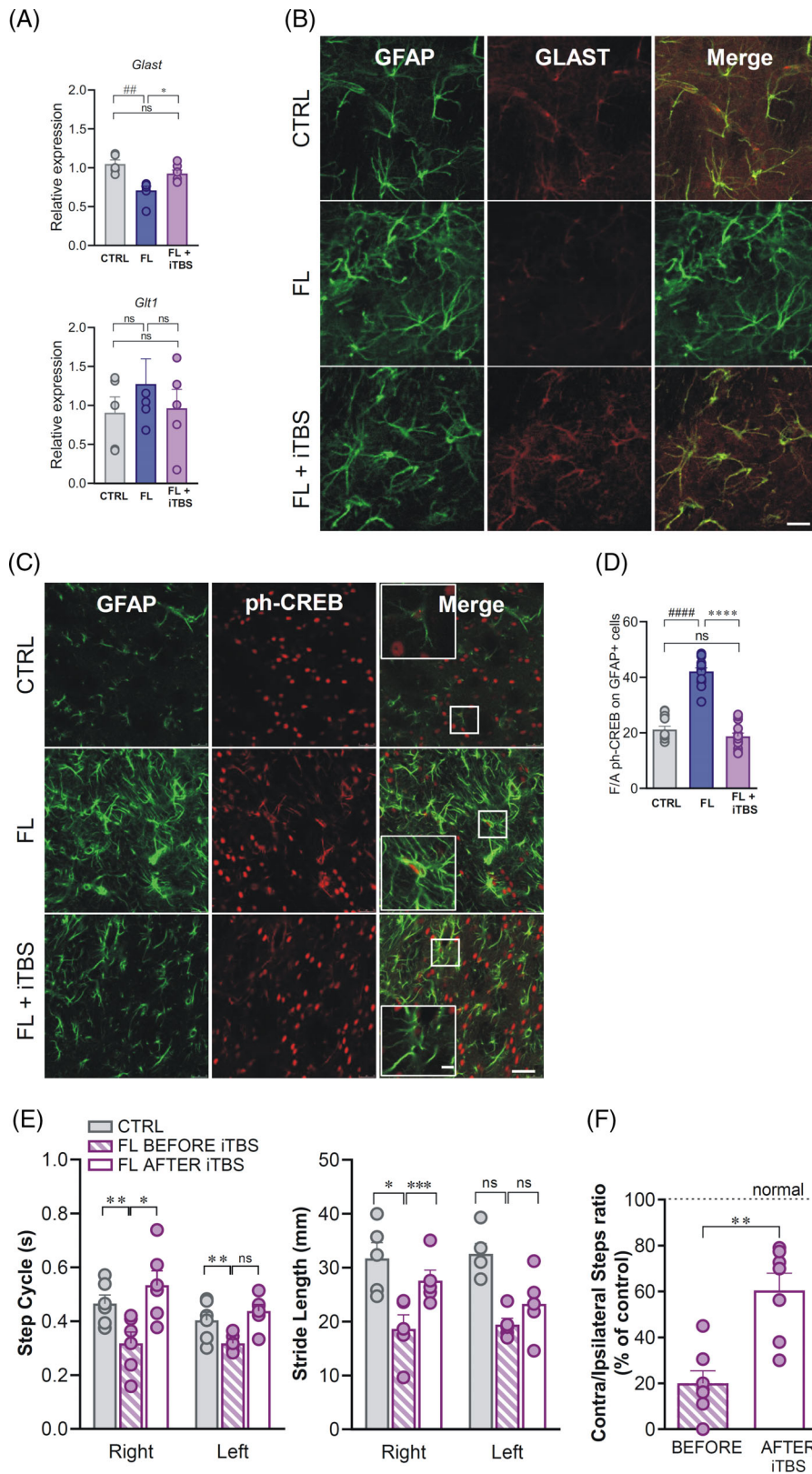


FIG. 4. Effects of intermittent theta-burst stimulation (iTBS) on glutamate–aspartate transporter (*Glust*) and glutamate transporter-1 (*Glt1*) mRNA levels, CREB activity and motor performances in parkinsonian animals. (A) Bar graph of *Glust* and *Glt1* relative expression in sham operated (CTRL), fully lesioned (FL), and FL + iTBS groups ($^{ns}P > 0.05$, $^{*}P < 0.05$, $^{##}P < 0.01$). (B) Representative confocal images of glial fibrillary acidic protein (GFAP) (green) and GLAST (red) immunostaining in the striatum of all different experimental conditions. Scale bar, 25 μ m. (C) Representative confocal images of GFAP

FIG. 4. Legend on next page.

This aligns with previous findings showing that the loss of dopamine-dependent plasticity in experimental parkinsonism, is associated with increased spontaneous glutamatergic activity and transmission in the striatum,^{14,50,51} but not reported in the hippocampus.

Another finding is that, within the striatum, the astrocytes display the most remarkable changes in response to iTBS. Neuromodulation through iTBS reduces 6-OHDA-induced astrogliosis and increases c-Fos expression in neurons¹³ and glial cells, with a marked effect on striatal astrocytes. Given the nature of immediate-early and transient genes expression, c-FOS-positive astrocytes found increased after iTBS may represent a functionally defined subset of astrocytes—probably at an intermediate/transition state between quiescent and reactive astrocytes—able to restore the striatal microenvironment homeostasis. Although this hypothesis requires additional investigation, it agrees with the synaptic role of astrocytes in limiting the excess of glutamate and with previous data showing a significant reduction of spontaneous glutamatergic activity in fully and partially lesioned parkinsonian animals subjected to acute iTBS.¹⁴ Here, we further explored the determinants potentially responsible for this recovery, showing that striatal GLAST, a key glial transporter in the reuptake of glutamate, was remarkably reduced in the parkinsonian animals and that acute iTBS was restored it. In addition, our results show that the decrease in GLAST mRNA and protein levels after dopamine denervation is associated with increased CREB phosphorylation in astrocytes. After iTBS, instead, GLAST upregulation correlated with reduced ph-CREB, consistent with the finding that GLAST is negatively regulated, at the transcriptional level, by ph-CREB.⁵⁷ Therefore, our results support the notion that iTBS, by regulating phosphorylation, might modulate astrocytes' ability to buffer excessive glutamate levels in the corticostriatal synapses of parkinsonian animals, extending previous findings.^{58,59} However, because a significant number of soluble factors and/or cAMP-dependent signaling elements can modulate the expression of *Glaxt*,⁵⁷ the role of specific signaling pathways triggered by 6-OHDA injury needs further investigation.

These changes in the glial reactivity were associated with improved striatal control of voluntary movements, as suggested by the reduction of forelimb akinesia and the rescue of motor skills necessary to learn how to

cross a confined walkway, an activity that, for unilaterally lesioned animals, whose tendency is to rotate in a challenging environment, requires a complete reorganization of the striatal control of body movements. Here, we also provide a methodological innovation by proposing more precise modeling of the animal brain over simplified spherical models, as supported by recent literature.^{60,61} Our computational model merged the already highly detailed ViZOO rat,³¹ counting 51 different structures with the 3D Waxholm Space atlas of a rat brain (RRID: SCR_01712).^{32,33} As this latter counts more than 200 separate brain regions and functional areas, such a reconstructed rat model allowed us to account for a hyper-realistic level of detail that goes far beyond what was considered in literature until now.^{60,61} It also allowed us to perform a highly accurate EM dosimetry that provides quantification of the TMS-induced E-field in separate specific brain regions known to be prone to synaptic plasticity (ie, hippocampus, striatum, and cerebellum). These results predicted that despite a whole-brain magnetic stimulation, each individual region is induced with different E-field intensity ($E_{\text{mean,hippocampus}} \sim 40$ V/m, $E_{\text{mean,striatum}} \sim 30$ V/m, $E_{\text{mean,cerebellum}} \sim 25$ V/m), which prompted us to further investigate the morphological changes in the glial cells of the three areas. Notably, among them, only the striatum showed alterations of the glial populations that were reverted by iTBS. These findings are in line with the reduced dispersion of the E-field in the striatum compared to the other areas. Such a compact response, because of the combination of anatomical characteristics and distance from the coil, might explain why in our setting, striatal astrocytes, which are robustly interconnected through gap junctions, seem to respond more actively to TMS.

For all these aspects, our results might be worthy of consideration from a translational perspective as the field of neuroimaging for in vivo visualization of reactive astrocytes is rapidly evolving.⁶² This relatively young field of research is opening new avenues to identify biomarkers related to PD progression⁶³ and outline clinical phenotypes in different neurodegenerative disorders.⁶⁴

Conclusions

With these findings, we uncovered a previously unknown effect of TMS on astrocyte modulation,

(green) and phospho-CREB (red) immunostaining in the striatum of CTRL, FL, and FL + iTBS animals. Scale bar, 25 μm ; insets, scale bar, 15 μm . (D) Bar graph of optical density (O.D.) of phospho-CREB in GFAP+ astrocytes in the different experimental conditions ($^{\#}P > 0.05$, $^{\#\#\#}$, $^{\#\#\#\#} P < 0.001$). (E) Histograms show averaged values of Step Cycle (left panel) and Stride Length (right panel) measured in CTRL and parkinsonian animals before (FL BEFORE iTBS) and after (FL AFTER iTBS), acute iTBS treatment, displaying a complete recovery of the right paw movements (Step Cycle $^*P < 0.05$; Stride Length $^{\#\#\#}P < 0.001$), altered after the lesion (Step Cycle $^{\#\#\#}P < 0.01$; Stride Length $^*P < 0.05$). (F) Histogram shows the averaged ratio, between the number of contralateral and ipsilateral steps made by FL exposed to iTBS expressed as a percent of control ($^{\#\#\#}P < 0.01$). Values are indicated as mean \pm standard error of the mean.

advancing our understanding of the mechanisms underlying iTBS-mediated neuroprotection.

We also generated a merged hyper-realistic rat model that provided the distribution of the electromagnetic quantities induced in specific brain areas. The results estimated are consistent with the experimental data, providing groundwork for a model-guided development of efficient magnetic stimulators.

Although the realization of a miniaturized coil was a too premature goal and not the remit of the current study, with these data, we established a principle for future studies to interrogate how the TMS-induced E-fields modulate distinct brain areas.

Although numerous additional features could be further investigated, here, we pinpointed the importance of conducting a dosimetric analysis to accompany *in vivo* experiments by exploiting existing highly detailed 3D-brain atlas, such as the Waxholm Space here considered. This combined approach would allow the researchers to better correlate their results with the TMS-induced E-field intensities, providing new insights into the potential of TMS as a therapeutic tool and indications for implementing TMS coils for preclinical investigations. ■

Acknowledgments: We thank ZMT Zurich MedTech, AG for providing licenses of the simulation software Sim4Life. Furthermore, we wish to acknowledge the Waxholm Space atlas of the Sprague Dawley rat brain, licensed under the Creative Commons Attribution ShareAlike (CC BY-SA) 4.0 license: <https://creativecommons.org/licenses/by-sa/4.0/>, made available through the INCF Software Center (<https://www.nitrc.org/projects/whs-sd-atlas>). Open access funding provided by BIBLIOSAN.

Data Availability Statement

The data that support the findings of this study are available from the corresponding author upon reasonable request.

References

1. Terao Y, Ugawa Y. Basic mechanisms of TMS. *J Clin Neurophysiol* 2002;19(4):322–343.
2. Lefaucheur JP, Aleman A, Baeken C, et al. Evidence-based guidelines on the therapeutic use of repetitive transcranial magnetic stimulation (rTMS): an update (2014–2018). *Clin Neurophysiol* 2020;131(2):474–528.
3. Wagner T, Valero-Cabre A, Pascual-Leone A. Noninvasive human brain stimulation. *Annu Rev Biomed Eng* 2007;9:527–565.
4. Cárdenas-Morales L, Volz LJ, Michely J, et al. Network connectivity and individual responses to brain stimulation in the human motor system. *Cereb Cortex* 2014;24(7):1697–1707.
5. Valero-Cabré A, Amengual JL, Stengel C, Pascual-Leone A, Coubard OA. Transcranial magnetic stimulation in basic and clinical neuroscience: a comprehensive review of fundamental principles and novel insights. *Neurosci Biobehav Rev* 2017;83:381–404.
6. Lefaucheur JP, André-Obadia N, Antal A, et al. Evidence-based guidelines on the therapeutic use of repetitive transcranial magnetic stimulation (rTMS). *Clin Neurophysiol* 2014;125(11):2150–2206.
7. Fried PJ, Jannati A, Davila-Pérez P, Pascual-Leone A. Reproducibility of single-pulse, paired-pulse, and intermittent theta-burst TMS measures in healthy aging, Type-2 diabetes, and Alzheimer's disease. *Front Aging Neurosci* 2017;9:263.
8. Di Lazzaro V, Rothwell J, Capogna M. Noninvasive stimulation of the human brain: activation of multiple cortical circuits. *Neuroscientist* 2018;24(3):246–260.
9. Strafella AP, Paus T, Barrett J, Dagher A. Repetitive transcranial magnetic stimulation of the human prefrontal cortex induces dopamine release in the caudate nucleus. *J Neurosci* 2001;21(15):RC157.
10. Madrid J, Benninger DH. Non-invasive brain stimulation for Parkinson's disease: clinical evidence, latest concepts and future goals: a systematic review. *J Neurosci Methods* 2021;347:108957.
11. Yang C, Guo Z, Peng H, et al. Repetitive transcranial magnetic stimulation therapy for motor recovery in Parkinson's disease: a meta-analysis. *Brain Behav* 2018;8(11):e01132.
12. Yue L, Xiao-lin H, Tao S. The effects of chronic repetitive transcranial magnetic stimulation on glutamate and gamma-aminobutyric acid in rat brain. *Brain Res* 2009;1260:94–99.
13. Cacace F, Mineo D, Viscomi MT, et al. Intermittent theta-burst stimulation rescues dopamine-dependent corticostriatal synaptic plasticity and motor behavior in experimental parkinsonism: possible role of glial activity. *Mov Disord* 2017;32(7):1035–1046.
14. Natale G, Pignataro A, Marino G, et al. Transcranial magnetic stimulation exerts "rejuvenation" effects on Corticostriatal synapses after partial dopamine depletion. *Mov Disord* 2021;36(10):2254–2263.
15. Wang HY, Crupi D, Liu J, et al. Repetitive transcranial magnetic stimulation enhances BDNF-TrkB signaling in both brain and lymphocyte. *J Neurosci* 2011;31(30):11044–11054.
16. Ba M, Kong M, Guan L, Yi M, Zhang H. Repetitive transcranial magnetic stimulation (rTMS) improves behavioral and biochemical deficits in levodopa-induced dyskinetic rats model. *Oncotarget* 2016;7(37):58802–58812.
17. Trippe J, Mix A, Aydin-Abidin S, Funke K, Benali A. θ burst and conventional low-frequency rTMS differentially affect GABAergic neurotransmission in the rat cortex. *Exp Brain Res* 2009;199(3–4):411–421.
18. Benali A, Trippe J, Weiler E, et al. Theta-burst transcranial magnetic stimulation alters cortical inhibition. *J Neurosci* 2011;31(4):1193–1203.
19. Clarke D, Penrose MA, Penstone T, et al. Frequency-specific effects of repetitive magnetic stimulation on primary astrocyte cultures. *Restor Neurol Neurosci* 2017;35(6):557–569.
20. Cullen CL, Young KM. How does transcranial magnetic stimulation influence glial cells in the central nervous system? *Front Neural Circuits* 2016;10:26.
21. Gellner AK, Reis J, Fritsch B. Glia: a neglected player in non-invasive direct current brain stimulation. *Front Cell Neurosci* 2016;10:188.
22. Clarke D, Beros J, Bates KA, Harvey AR, Tang AD, Rodger J. Low intensity repetitive magnetic stimulation reduces expression of genes related to inflammation and calcium signalling in cultured mouse cortical astrocytes. *Brain Stimul* 2021;14(1):183–191.
23. Hong Y, Liu Q, Peng M, et al. High-frequency repetitive transcranial magnetic stimulation improves functional recovery by inhibiting neurotoxic polarization of astrocytes in ischemic rats. *J Neuroinflammation* 2020;17(1):150.
24. Sofroniew MV, Vinters HV. Astrocytes: biology and pathology. *Acta Neuropathol* 2010;119(1):7–35.
25. Anderson CM, Swanson RA. Astrocyte glutamate transport: review of properties, regulation, and physiological functions. *Glia* 2000;32(1):1–14.
26. Sheldon AL, Robinson MB. The role of glutamate transporters in neurodegenerative diseases and potential opportunities for intervention. *Neurochem Int* 2007;51(6–7):333–355.
27. Chotibut T, Davis RW, Arnold JC, et al. Ceftriaxone increases glutamate uptake and reduces striatal tyrosine hydroxylase loss in 6-OHDA Parkinson's model. *Mol Neurobiol* 2014;49(3):1282–1292.
28. Chung EK, Chen LW, Chan YS, Yung KK. Downregulation of glial glutamate transporters after dopamine denervation in the striatum

- of 6-hydroxydopamine-lesioned rats. *J Comp Neurol* 2008;511(4):421–437.
29. Iovino L, Tremblay ME, Civiero L. Glutamate-induced excitotoxicity in Parkinson's disease: the role of glial cells. *J Pharmacol Sci* 2020;144(3):151–164.
 30. Ghiglieri V, Pendolino V, Sgobio C, Bagetta V, Picconi B, Calabresi P. Θ -burst stimulation and striatal plasticity in experimental parkinsonism. *Exp Neurol* 2012;236(2):395–398.
 31. Kainz W, Nikoloski N, Oesch W, et al. Development of novel whole-body exposure setups for rats providing high efficiency, National Toxicology Program (NTP) compatibility and well-characterized exposure. *Phys Med Biol* 2006;51(20):S211–S229.
 32. Papp EA, Leergaard TB, Calabrese E, Johnson GA, Bjaalie JG. Waxholm space atlas of the Sprague Dawley rat brain. *Neuroimage* 2014;97:374–386.
 33. Leergaard TB, Kleven H, Clascá F, et al. Waxholm space atlas of the rat brain: a 3D atlas supporting data analysis and integration. *Research Square* 2023. <https://doi.org/10.21203/rs.3.rs-2466303/v1>
 34. Colella M, Paffi A, De Santis V, Apollonio F, Liberti M. Effect of skin conductivity on the electric field induced by transcranial stimulation techniques in different head models. *Phys Med Biol* 2021;66(3):035010.
 35. Thielscher A, Kammer T. Electric field properties of two commercial figure-8 coils in TMS: calculation of focality and efficiency. *Clin Neurophysiol* 2004;115(7):1697–1708.
 36. Bungert A, Antunes A, Espenhahn S, Thielscher A. Where does TMS stimulate the motor cortex? Combining electrophysiological measurements and realistic field estimates to reveal the affected cortex position. *Cereb Cortex* 2017;27(11):5083–5094.
 37. Laakso I, Murakami T, Hirata A, Ugawa Y. Where and what TMS activates: experiments and modeling. *Brain Stimul* 2018;11(1):166–174.
 38. Weise K, Numssen O, Thielscher A, Hartwigsen G, Knösche TR. A novel approach to localize cortical TMS effects. *Neuroimage* 2020;209:116486.
 39. Paffi ACF, Carducci F, Rubino G, Tampieri P, Liberti M, Apollonio F. A computational model for real-time calculation of electric field due to transcranial magnetic stimulation in clinics. *Int J Antennas Propagation* 2015;2015:1–11. <https://doi.org/10.1155/2015/976854>
 40. Ghiglieri V, Mineo D, Vannelli A, et al. Modulation of serotonergic transmission by eltopazine in L-DOPA-induced dyskinesia: behavioral, molecular, and synaptic mechanisms. *Neurobiol Dis* 2016;86:140–153.
 41. Viscomi MT, Florenzano F, Latini L, Amantea D, Bernardi G, Molinari M. Methylprednisolone treatment delays remote cell death after focal brain lesion. *Neuroscience* 2008;154(4):1267–1282.
 42. Catale C, Bisicchia E, Carola V, Viscomi MT. Early life stress exposure worsens adult remote microglia activation, neuronal death, and functional recovery after focal brain injury. *Brain Behav Immun* 2021;94:89–103.
 43. Botta-Dukát Z. Quartile coefficient of variation is more robust than CV for traits calculated as a ratio. *Sci Rep* 2023;13(1):4671.
 44. Gomez LJ, Dannhauer M, Koponen LM, Peterchev AV. Conditions for numerically accurate TMS electric field simulation. *Brain Stimul* 2020;13(1):157–166.
 45. Moretti J, Terstege DJ, Poh EZ, Epp JR, Rodger J. Low intensity repetitive transcranial magnetic stimulation modulates brain-wide functional connectivity to promote anti-correlated c-Fos expression. *Sci Rep* 2022;12(1):20571.
 46. Costa C, Sgobio C, Siliquini S, et al. Mechanisms underlying the impairment of hippocampal long-term potentiation and memory in experimental Parkinson's disease. *Brain* 2012;135(6):1884–1899.
 47. Sasso V, Bisicchia E, Latini L, et al. Repetitive transcranial magnetic stimulation reduces remote apoptotic cell death and inflammation after focal brain injury. *J Neuroinflammation* 2016;13(1):150.
 48. Matos M, Augusto E, Oliveira CR, Agostinho P. Amyloid-beta peptide decreases glutamate uptake in cultured astrocytes: involvement of oxidative stress and mitogen-activated protein kinase cascades. *Neuroscience* 2008;156(4):898–910.
 49. Lee E, Sidoryk-Węgrzynowicz M, Wang N, et al. GPR30 regulates glutamate transporter GLT-1 expression in rat primary astrocytes. *J Biol Chem* 2012;287(32):26817–26828.
 50. Bagetta V, Sgobio C, Pendolino V, et al. Rebalance of striatal NMDA/AMPA receptor ratio underlies the reduced emergence of dyskinesia during D2-like dopamine agonist treatment in experimental Parkinson's disease. *J Neurosci* 2012;32(49):17921–17931.
 51. Calabresi P, Mercuri NB, Sancesario G, Bernardi G. Electrophysiology of dopamine-denervated striatal neurons. *Implicat Parkinson's Dis Brain* 1993;116(2):433–452.
 52. Campanelli F, Natale G, Marino G, Ghiglieri V, Calabresi P. Striatal glutamatergic hyperactivity in Parkinson's disease. *Neurobiol Dis* 2022;168:105697.
 53. Mathur BN, Lovinger DM. Endocannabinoid-dopamine interactions in striatal synaptic plasticity. *Front Pharmacol* 2012;3:66.
 54. Yin HH, Lovinger DM. Frequency-specific and D2 receptor-mediated inhibition of glutamate release by retrograde endocannabinoid signaling. *Proc Natl Acad Sci U S A* 2006;103(21):8251–8256.
 55. Covelo A, Eraso-Pichot A, Fernandez-Moncada I, Serrat R, Marsicano G. CB1R-dependent regulation of astrocyte physiology and astrocyte-neuron interactions. *Neuropharmacology* 2021;195:108678.
 56. Eraso-Pichot A, Pouvreau S, Olivera-Pinto A, Gomez-Sotres P, Skupio U, Marsicano G. Endocannabinoid signaling in astrocytes. *Glia* 2023;71(1):44–59.
 57. Gegelashvili G, Dehnes Y, Danbolt NC, Schousboe A. The high-affinity glutamate transporters GLT1, GLAST, and EAAT4 are regulated via different signalling mechanisms. *Neurochem Int* 2000;37(2–3):163–170.
 58. Kim SY, Choi SY, Chao W, Volsky DJ. Transcriptional regulation of human excitatory amino acid transporter 1 (EAAT1): cloning of the EAAT1 promoter and characterization of its basal and inducible activity in human astrocytes. *J Neurochem* 2003;87(6):1485–1498.
 59. Liu YP, Yang CS, Tzeng SF. Inhibitory regulation of glutamate aspartate transporter (GLAST) expression in astrocytes by cadmium-induced calcium influx. *J Neurochem* 2008;105(1):137–150.
 60. Koponen LM, Stenroos M, Nieminen JO, Jokivarsi K, Gröhn O, Ilmoniemi RJ. Individual head models for estimating the TMS-induced electric field in rat brain. *Sci Rep* 2020;10(1):17397.
 61. Boonzaier J, Petrov PI, Otte WM, Smirnov N, Neggers SFW, Dijkhuizen RM. Design and evaluation of a rodent-specific transcranial magnetic stimulation coil: an In Silico and In vivo validation study. *Neuromodulation* 2020;23(3):324–334.
 62. Harada R, Furumoto S, Kudo Y, Yanai K, Villemagne VL, Okamura N. Imaging of reactive astroglia by positron emission tomography. *Front Neurosci* 2022;16:807435.
 63. Wilson H, Dervenoulas G, Pagano G, et al. Imidazole 2 binding sites reflecting astroglia pathology in Parkinson's disease: an in vivo ¹¹C-BU99008 PET study. *Brain* 2019;142(10):3116–3128.
 64. Liu Y, Jiang H, Qin X, Tian M, Zhang H. PET imaging of reactive astrocytes in neurological disorders. *Eur J Nucl Med Mol Imaging* 2022;49(4):1275–1287.

Supporting Data

Additional Supporting Information may be found in the online version of this article at the publisher's web-site.